

Design and Validation of a Microfluidic Chip for the Circulating Tumor Cells Sorting based on Electrophoretic Technology

Jingye Li^{1,*}, Zhigang Hu^{1,2}, Xiangyang Zu², Kena Song²

¹College of Mechanical and Electrical Engineering, Henan University of Science and Technology, Luoyang 471003, China

²College of Medical Technology and Engineering, Henan University of Science and Technology, Luoyang 471003, China

*Correspondence: lijingye1001@163.com

Abstract

Circulating tumor cells (CTCs) are a collective term for various types of tumor cells in peripheral blood, and their presence in peripheral blood is an important indicator for detecting malignant tumors. In this study, we designed a three-dimensional CTCs sorting chip with serrated electrode pattern based on the principle of dielectrophoresis, which utilized the differences between CTCs and leukocytes in terms of dielectric properties and movement trajectories to achieve the separation and enrichment of CTCs. Moreover, the three-dimensional chip exhibits a higher channel capacity, which allows for greater sample throughput and scalability. This increased channel capacity facilitates more effective sorting of particles or cells, resulting in a superior sorting effect compared to the rectangular shape commonly used in two-dimensional chips. The serrated electrode pattern in the three-dimensional chip contributes to this improved sorting capability. Firstly, we constructed a three-dimensional sorting model using COMSOL software and simulated the cell motion trajectory to establish the simulation parameters for the subsequent experiments. Secondly, laser etching and plasma bonding techniques were utilized to prepare the chip and establish the experimental platform for microfluidic cell sorting. Finally, human breast cancer cells MDA-MB-231 were used as the experimental objects, and the separation and enrichment experiments were carried out on the chip. Results show the results showed that the maximum separation flux of human breast cancer cells MDA-MB-231 on the microfluidic chip was 2.0 mL/h under the condition of voltage of 10Vrms and frequency of 210kHz, and the optimal separation efficiency reached 90%. Conclusion This study has important reference value for the enrichment, sorting and detection of circulating tumor cells.

Keywords

Dielectrophoresis; Circulating tumor cell sorting; Simulation experiment; Microfluidic chip.

1. INTRODUCTION

Circulating tumor cells (CTCs), which are tumor cells that detach from the primary tumor and enter the bloodstream, survive in the circulatory system and eventually metastasize [1]. They can be detected through blood tests. It is estimated that 90% of cancer-related deaths in tumor patients are caused by metastasis, highlighting the critical importance of early diagnosis and treatment to improve therapeutic outcomes[2]. Each milliliter of peripheral blood contains approximately 1-100 CTCs[3], a remarkably sparse quantity compared to other cells in the

blood such as leukocytes (10^6) and red blood cells (10^9). Consequently, efficient and high-purity enrichment of CTCs from peripheral blood has become a major focus and hotspot in the field of circulating tumor cell enrichment and detection techniques [4].

Detection techniques for CTCs are primarily based on enrichment methods. Common enrichment methods for CTCs include physical methods based on biophysical characteristics such as size, density, deformability, and electrical properties[5-7], as well as biochemical methods based on the highly specific interaction between ligands on the CTCs' cell membrane and tumor-specific antigens[8,9]. Among them, electrophoretic enrichment technology (also known as dielectrophoresis or bidirectional electrophoretic enrichment technology)[10] is a biophysical-based enrichment method that utilizes the differences in magnitude and direction of electric field forces experienced by cells in a non-uniform electric field to drive cell movement in a specific direction. Compared to other enrichment methods, dielectrophoresis-based technology utilizes the inherent electrical properties of circulating tumor cells (CTCs), eliminating the need for labeling. This technique offers advantages such as minimal cell damage, cost-effectiveness, rapidity, high sensitivity and selectivity. Microelectrode-based electrophoretic enrichment devices can be classified into parallel or interdigitated types [11], sawtooth types [12], tilted types [13], curved types [14], quadrupole types [15], microwell types [16], rectangular types [17], top-bottom pattern types [18], and sidewall pattern types [19], among others.

This study presents the design of an upper and lower patterned dielectrophoresis chip, consisting of three main components: a bottom plate with a serrated electrode pattern[20], a microchannel layer, and a cover plate made of conductive glass. The overall structure is illustrated in Figure 1a by applying a signal of specific frequency to the chip using a signal generator, circulating tumor cells experience a positive dielectrophoretic force and are selectively adsorbed onto the bottom electrode, while other cells experience a negative dielectrophoretic force and are carried away by the suspension fluid, thus completing the sorting process. The principle of chip separation is depicted in Figure 1b.

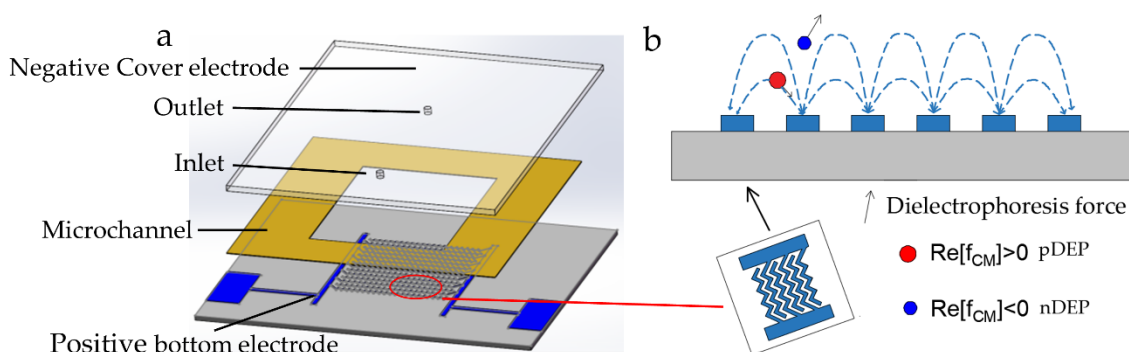


Figure 1. (a) Schematic diagram of the chip structure. The three-dimensional dielectrophoresis microfluidic chip consists of three layers: the cover plate (white region), the rectangular main channel (yellow region), and the bottom plate (blue region) with serrated interdigitated electrodes. Both the cover plate and bottom plate are made of ITO glass, while the channel portion is composed of a PDMS membrane.; (b) Schematic diagram of the chip separation principle. The blue lines represent the electric field lines, and the enlarged diagram of the serrated electrode in the bottom left corner is shown in Figure A. The red spheres depict the force exerted on breast cancer cells, while the blue spheres represent white blood cells.

Table 1. Table of parameters for the CTCs sorting model.

Symbols	Describe	Parameters
f_0	crossover frequency	210kHz
σ_f	Conductivity of fluid medium	550 μ s/cm
ε_f	Dielectric constant of fluid	80
ρ_f	Fluid density	1000kg/m ³
μ_f	Membrane dynamic viscosity	5 Pa*s
ρ_p	Grain density	1050kg/m ³
r_1	Breast cancer cell size	6.2 μ m
r_2	Leukocyte size	4.7 μ m
σ_{p1}	Breast cancer cell conductivity	0.62 S/m
σ_{p2}	White blood cell conductivity	0.6 S/m
ε_{p1}	Relative dielectric constant of breast cancer cells	52
ε_{p2}	Relative dielectric constant of leukocyte	151

2. MATERIALS AND METHODS

2.1. Theoretical basis

Dielectrophoresis (DEP) is a phenomenon in which neutral particles in a fluid, under the influence of a non-uniform electric field, experience induced polarization due to their different polarizability from the surrounding medium. This results in a positive or negative motion effect towards the electric field gradient [21]. If the particle has a higher polarizability than the suspension fluid, it will experience positive dielectrophoretic force (pDEP) and move towards regions of higher electric field. On the other hand, if the particle has a lower polarizability than the surrounding medium, it will experience negative dielectrophoretic force (nDEP) and move towards regions of lower electric field. In a sinusoidally varying non-uniform electric field, the magnitude of the dielectrophoretic force acting on the particle is given by the formula:

$$F_{DEP} = 2\pi\varepsilon_m r^3 \operatorname{Re}[K(\omega)] \nabla E_{rms}^2 \quad (1)$$

Where ε_m represents the dielectric constant of the solution, r represents the particle radius, E is the electric field gradient; ω is the angular frequency of the AC signal, $K(\omega)$ represents the Clausius-Mossotti factor [22], also known as the CM factor. The real part of the CM factor, $\operatorname{Re}[K(\omega)]$, determines the positive or negative nature of the dielectrophoretic force.

The expression for $K(\omega)$ is:

$$K(\omega) = \frac{\varepsilon_p^* - \varepsilon_m^*}{\varepsilon_p^* + 2\varepsilon_m^*} \quad (2)$$

$$\varepsilon_p^* = \varepsilon_p - j \frac{\sigma_p}{\omega} \quad (3)$$

$$\varepsilon_m^* = \varepsilon_m - j \frac{\sigma_m}{\omega} \quad (4)$$

$$\begin{aligned} \operatorname{Re}[K(\omega)] &= \operatorname{Re}\left(\frac{\varepsilon_p^* - \varepsilon_m^*}{\varepsilon_p^* + 2\varepsilon_m^*}\right) = \\ &= \frac{\omega^2(\varepsilon_p - \varepsilon_m)(\varepsilon_p + 2\varepsilon_m) - (\sigma_m - \sigma_p)(2\sigma_m + \sigma_p)}{\omega^2(\varepsilon_p + 2\varepsilon_m)^2 + (2\sigma_m + \sigma_p)^2} \end{aligned} \quad (5)$$

Where: $j = \sqrt{-1}$; $\operatorname{Re}[K(\omega)]$ is the real part of the CM factor, and the range of values is $[-0.5 \sim 1]$. ε_p is the permittivity of the particle; ε_m^* and ε_p^* are the complex permittivity of the solution and the particle; σ_m and σ_p are the conductivity of the solution and the particle, respectively. The permittivity of the solution and the particle determine the positive and negative $\operatorname{Re}[K(\omega)]$, and the positive and negative $\operatorname{Re}[K(\omega)]$ determine the direction of the dielectrophoretic force. When $\operatorname{Re}[K(\omega)] > 0$, the particle will be subjected to positive dielectrophoretic force (pDEP) and move in the direction of high electric field; when $\operatorname{Re}[K(\omega)] < 0$, the particle will be subjected to negative dielectrophoretic force (nDEP) and move in the direction of low electric field. when $\operatorname{Re}[K(\omega)] = 0$, the dielectrophoretic force is zero, the particle is not affected by the electric field, and the frequency at this time is called the cross frequency.

Electrode shape, main channel height and microelectrode voltage alter the cell movement trajectory by affecting the electric field inside the chip. And the flow velocity produces changes to the cell motion trajectory mainly by affecting the Stokes force in the fluid. Therefore, the simulation modeling includes electrode pattern shape, main channel height, microelectrode voltage and flow velocity.

2.2. Model building and numerical simulation

A 3D model of sawtooth electrode simulation using SolidWorks software was imported into COMSOL Multiphysics 5.5 software, and the AC/DC module, laminar flow module and fluid flow particle tracking module of the software were utilized. The separation process of CTCs (breast cancer cells) and leukocytes was simulated by calculating the electric field, flow field and particle trajectory problems. In this paper, the simulated cells are breast cancer cells MDA-MB-231 (red) and leukocytes (blue). The crossover frequencies of breast cancer cells MDA-MB-231 and leukocytes were 180 kHz and 210 kHz, respectively, at a conductivity of 550 $\mu\text{s}/\text{cm}$. To ensure that breast cancer cells MDA-MB-231 were subjected to sufficiently large positive dielectrophoretic forces and leukocytes were subjected to negative dielectrophoretic forces, 210 kHz, which was closer to the crossover frequency of leukocytes, was chosen as the frequency of simulation. The model's parameters are shown in Table 1, and the optimal parameters for chip cell separation were determined by simulation optimization of electrode shape and channel height, chip voltage, and flow rate. Through simulation optimization of chip voltage, channel height, and flow rate, the optimal parameters for cell separation in the chip were determined.

2.3. Microfluidic chip physical processing

The chip fabrication process consists of three main steps: design and preparation of microelectrodes, design and fabrication of microchannels, and bonding of electrodes and channels, followed by subsequent processing. In this study, a three-dimensional microelectrode design based on dielectrophoresis technology was employed, with the cover plate and bottom plate made of indium tin oxide (ITO) conductive glass, and the intermediate layer

microchannels made of polydimethylsiloxane (PDMS) thin film. ITO conductive glass was selected as the electrode material.

The fabrication method for etching the pattern on ITO conductive glass utilizes laser etching. The design pattern for the bottom plate electrodes is shown in Figure 2a the process for laser etching ITO conductive glass is as follows: (1) CAD design drafting; (2) Import the drafting; (3) Adjust machine parameters (first etch with faulty glass, then measure using a two-dimensional measuring instrument) (4) Initial inspection. (5) Begin etching.

The simulated microchannel had a height of $150\mu\text{m}$. As a material close to the simulated microchannel height, polymethyl methacrylate (PMMA) was chosen. However, PDMS has specific thickness requirements, with a minimum thickness of $200\mu\text{m}$. For this reason, KYN- $150\mu\text{m}$ PDMS provided by RiaThin Films was selected. Based on the shape of the microelectrode bottom plate, the microchannel was designed. The electrode area of the channel needed to be exposed for cell adsorption, and a certain width was required for bonding PDMS and glass. Therefore, a PDMS microchannel area with dimensions of $40\times 40\text{ mm}$ was designed, with a region of $10\times 25\text{ mm}$ etched in the middle to facilitate the generation of a non-uniform electric field between the upper and lower electrodes.

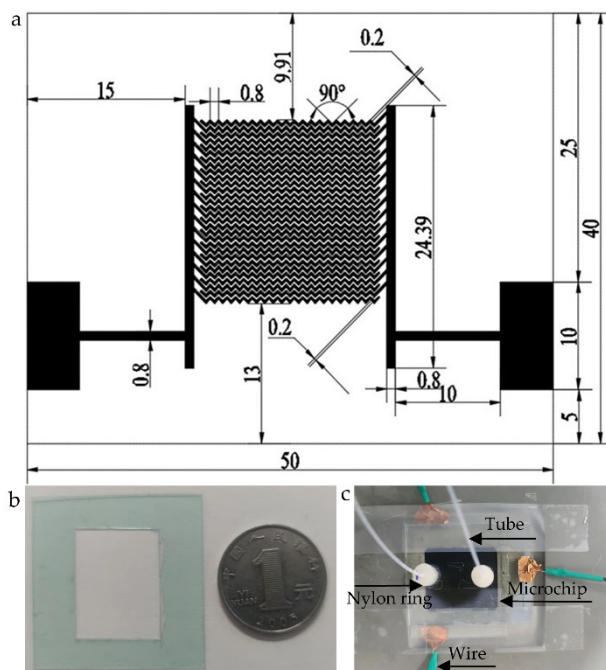


Figure 2. (a) Schematic diagram of the CTCs dielectrophoresis chip sorting model structure (scale mm); (b) Microchannel physical diagram; (c) Microfluidic chip physical diagram.

The bonding process of the microfluidic chip's electrodes and channels is as follows: (1) Set the parameters of the plasma cleaner to 30% power and clean for 20 seconds. (2) Place the electrode bottom plate and PDMS channel with the bonding surfaces facing up into the plasma cleaner. After cleaning, quickly remove them and align the PDMS with the electrode bottom plate, applying pressure. Then, place them in a 60°C drying oven for 5 minutes. (3) Repeat step 2, aligning the inlet and outlet of the cover plate electrode holes with the electrode area, and bond them onto the PDMS channel. Press the three-layer structure together quickly and place it in a 60°C drying oven for 20 minutes to achieve permanent bonding. To complete the setup, first, attach $0.5\times 0.9\text{ mm}$ PTFE tubing to the chip's inlet and outlet. Then, position a nylon ring above the tubing and firmly adhere it to the chip, ensuring a tight seal at the connection between the chip and tubing. Next, insert a conductive needle into the designated area on the electrode

bottom plate, securing it in place by using conductive adhesive tape. Finally, solder a wire to the opposite end of the conductive needle, providing an easy and reliable connection with the waveform generator. To mount the chip onto a microscope, fabricate a fixture using a CNC milling machine that perfectly matches the dimensions of the chip. The physical picture of the microchannel is shown in Figure 2b, the physical diagram of the microfluidic chip is shown in Figure 2c.

2.4. The construction of the CTCs sorting experimental platform

The following instruments were utilized in constructing the microfluidic experimental platform: an injection pump (Shenchen SPC split injection pump), a fluorescence microscope (Olympus IX53), an arbitrary waveform generator (Tektronix AFG3102), a digital oscilloscope (Tektronix TDS2002), syringes, a computer, as well as beakers and test tubes. The fluorescence microscope was connected to the computer for observing and collecting cell sorting images. The inlet of the chip was connected to the syringe through a Teflon tube, and the needle of the syringe was coated with adhesive to prevent leakage when injecting cell solution. The outlet tube was placed into a waste container. The chip was fixed on the microscope using a chip holder. After filling a 1ml syringe with laboratory water and connecting it to the needle on the chip, it was placed on the injection pump. The fluorescence microscope and white light laser were turned on, and the chip position was adjusted through bright field observation to ensure compatibility with the fluorescence microscope. The chip was then perfused with a flow rate of 10ml/h two to three times to clean the chip and prevent residual cells from adhering to the bottom plate, thus affecting the sorting efficiency. The schematic diagram of the sorting platform is shown in Figure 3.

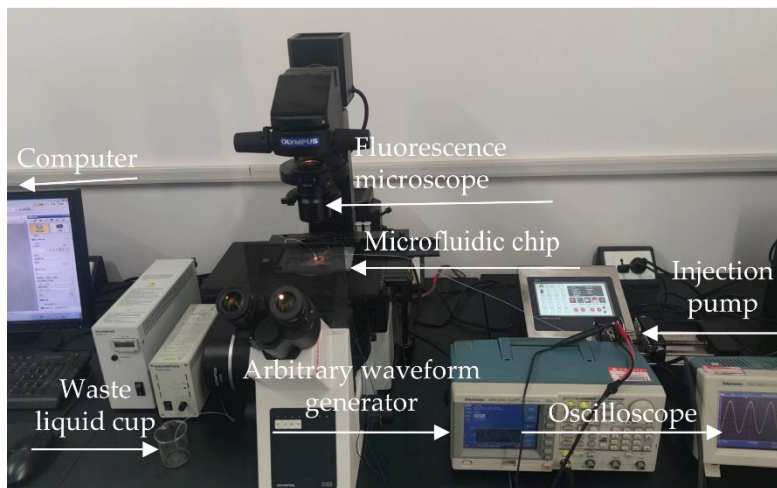


Figure 3. The schematic diagram of CTCs sorting platform.

3. RESULTS

3.1. Effect of electrode pattern and channel height on the sorting effect of CTCs

The electrode pattern will affect the electric field inside the chip and thus the sorting effect, we simulated the effect of rectangular and serrated electrodes on the sorting effect, and the results are shown in Fig. 4. In Figure 4, gray areas in the background are microfluidic channels, red microspheres indicate breast cancer cells, and blue microspheres indicate leukocytes. The lower part shows adsorbed cells and the right exit shows unsuccessfully adsorbed cells. Through observation, it was found that the number of red breast cancer cells adsorbed to the serrated electrode (Fig. b) was significantly more than that of the rectangular electrode (Fig. a), and many unadsorbed breast cancer cells of the rectangular electrode were gathered at the exit,

so the serrated electrode pattern was chosen as the electrode design diagram of the chip bottom plate.

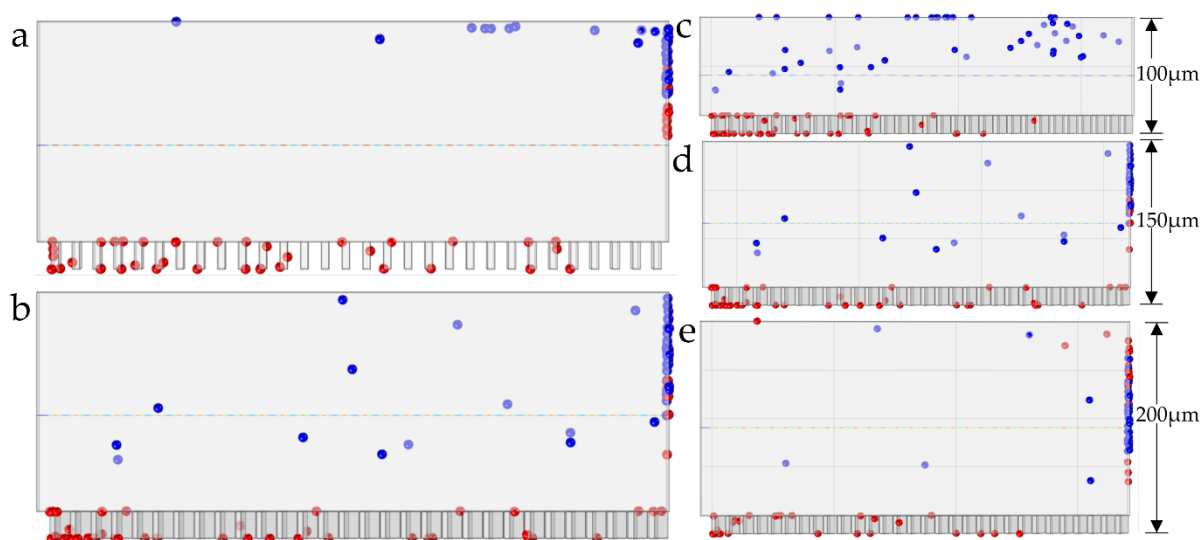


Figure 4. Sorting effect image of CTCs under the influence of electrode pattern and channel heights. (a) Cell sorting under rectangular electrodes pattern; (b) Cell sorting under serrated electrodes pattern; (c) Cell sorting under channel height of 100 μm ; (d) Cell sorting under channel height of 150 μm ; (e) Cell sorting under channel height of 200 μm .

The height of the microchannel can affect the amount of sample separated and the magnitude of the electric field within the chip. An increase in channel height leads to an increase in the amount of sample separated, but a decrease in the electric field strength and dielectrophoretic force. In order to determine the optimal value of the chip channel height, the cell sorting process under three standard sizes (100 μm , 150 μm , and 200 μm) of PDMS film was simulated in this paper, and the results are shown in Fig. 4. On the right side, the different channel heights of the three figures are labeled in μm . Through the simulation, it is found that the two kinds of cells have a better separation effect under the channel height of 150 μm when the frequency is 210 kHz and the conditions of potential difference and flow rate are the same. Compared with the channel height of 100 μm , the channel height of 150 μm has a larger separation volume and higher separation efficiency. When the channel height was increased to 200 μm , due to the insufficient dielectrophoretic force, some of the breast cancer cells would flow out with the decreased adsorption capacity of the microelectrode, which made the sorting effect decrease significantly. Considering the separation efficiency of CTCs, a channel height of 150 μm was selected as the design parameter of the dielectrophoresis chip.

3.2. Effect of microelectrode potential on the separation of CTCs

From equation (1) of electrophoretic force, it can be deduced that the greater the potential difference (∇E^2), the stronger the electrophoretic force generated within the chip. Under the given conditions of a frequency of 210kHz, electrode spacing of 200 μm , microchannel height of 150 μm , and flow rate of 370 $\mu\text{m}/\text{s}$, we varied the voltage applied to the top and bottom plate electrodes to determine the effect of electric field distribution on the sorting performance. The simulated sorting results are shown in Figure 5.

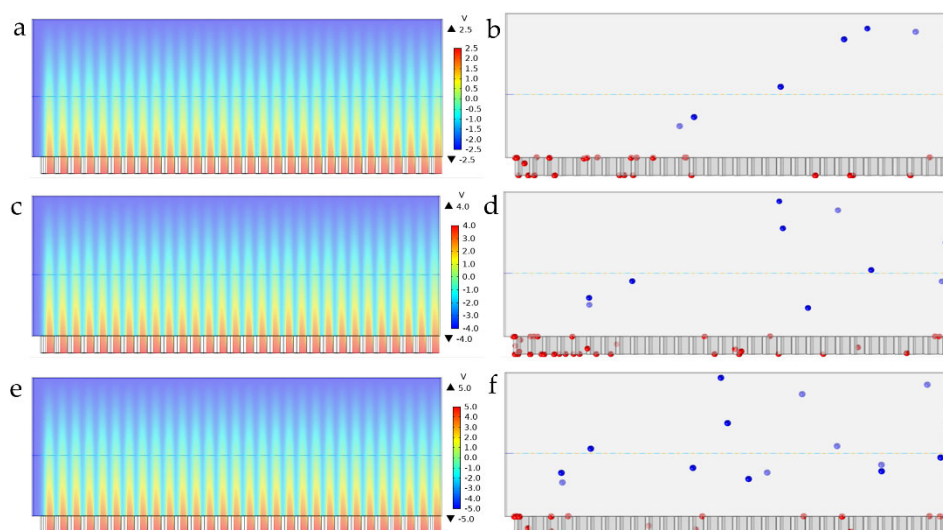


Figure 5. Electric field distribution and CTCs sorting result image. (a) The color legend on the right side identifies the maximum and minimum values of the voltage, the units and the distribution of the electric field. The legend corresponds to the color of the main picture, and the darker the color means the higher the voltage here. Electric field distribution at voltage 5v; (b) CTCs sorting effect diagram under 5V voltage; (c) Electric field distribution at voltage 8v; (d) CTCs sorting effect diagram under 8V voltage; (e) Electric field distribution at voltage 10v; (f) CTCs sorting effect diagram under 10V voltage.

The labels on the right side of Figure 6 indicate the distribution of the electric field, and the colors correspond to the images and labels. The gray-white background represents the flow field region. A low voltage is applied to the top plate, while a high voltage is applied to the bottom plate to create a potential difference. When a voltage difference of 5V is applied to the microelectrodes, as shown in Figure 5b some breast cancer cells fail to adhere effectively to the bottom plate and are carried away by the liquid flow. By increasing the voltage difference to 8V, as shown in Figure 6d there is a significant improvement in the sorting effect compared to 5V. The number of breast cancer cells adhering to the microelectrodes increases, while the number of non-adherent breast cancer cells gathering at the outlet decreases. Furthermore, by further increasing the voltage difference to 10V, as shown in Figure 6f the sorting effect is further enhanced. Therefore, based on these results, we conclude that within the allowable range of electrode etching processes, a higher voltage applied to the microelectrodes leads to better sorting performance. Consequently, we choose a potential difference of 10V as the voltage simulation condition.

3.3. Effect of flow rate on CTCs sorting effect

When separating CTC cells in the channel of the chip, both Stokes force and electrophoretic force are the main forces acting on the cells. The trajectory of cell movement is determined by the resultant force generated by these two forces. As the liquid flow rate increases due to the release from the injection pump, the Stokes force increases while the influence of the electrophoretic force on the cells decreases, thereby altering the simulated cell motion trajectory. Under the condition of keeping other parameters constant (frequency of 210kHz, electrode spacing of 200 μm , channel height of 150 μm , potential difference of 10V), we simulated the cell motion trajectories at three different flow rates, as shown in Figure 6.

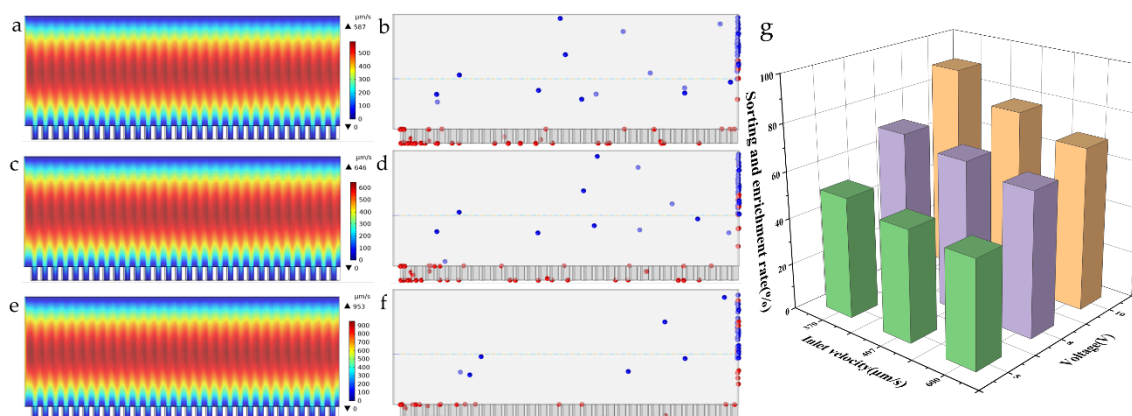


Figure 6. Flow field distribution and its sorting result image. (a) The color legend on the right side identifies the maximum and minimum values of the velocity, the units and the distribution of the flow field. The legend corresponds to the color of the main picture, and the darker the color means the faster the flow here. Flow field distribution at an inlet flow velocity of $370\mu\text{m/s}$; (b) CTCs sorting effect diagram under $370\mu\text{m/s}$; (c) Flow field distribution at an inlet flow velocity of $407\mu\text{m/s}$; (d) CTCs sorting effect diagram under $407\mu\text{m/s}$; (e) Flow field distribution at an inlet flow velocity of $600\mu\text{m/s}$; (f) CTCs sorting effect diagram under $600\mu\text{m/s}$; (g) Simulation parameters and characterization of sorting effectiveness chart.

The labels on the right side of the figure indicate the distribution of the flow field, corresponding to the colors on the left side. The inlet is located on the left, and the outlet is located on the right, with the fluid flowing from left to right. Under a flow rate of $370\mu\text{m/s}$, breast cancer cells and granulocytes are successfully separated, as shown in Figure 6b. However, as the flow rate increases, the position of breast cancer cell separation moves further away from the inlet and starts to accumulate at the outlet, as shown in Figure 6d. This is due to the increase in Stokes force while the electrophoretic force remains constant, resulting in a decrease in the adhesive effect on the bottom electrode plate. When we further increase the simulated flow rate to $600\mu\text{m/s}$, more breast cancer cells accumulate at the outlet, indicating a significant deterioration in the separation effect. The simulation results demonstrate that a higher flow rate leads to relatively poorer sorting performance. However, we still need to maximize the flow rate as much as possible to improve the separation efficiency. Therefore, considering the simulation results and without compromising the separation effect, we choose a flow rate of $370\mu\text{m/s}$ (2.0mL/h) as the optimal speed parameter. Figure 6g displays a characterization of the simulation parameters and the sorting performance. Simulation results demonstrate that under the conditions of a channel height of $150\mu\text{m}$, a voltage of 10V , and an inlet flow rate of $370\mu\text{m/s}$ (2.0mL/h), the sorting enrichment efficiency reaches an optimal value of 90%.

3.4. Microarray separation of human breast cancer cells MDA-MB-231 experiment

Using the constructed experimental platform for separation, we verified the actual separation and enrichment efficiency of circulating tumor cells (CTCs) on the chip, taking the human breast cancer cell line MDA-MB-231 as an example. The experiment was conducted under the conditions of a channel height of $150\mu\text{m}$ and a voltage of 10V ($\pm 5\text{Vrms}$). Subsequently, velocity parameter experiments were performed. The concentration of MDA-MB-231 cells in the solution was adjusted to 4×10^4 cells/mL using a cell counting plate and PBS buffer. 0.5ml of the pre-configured MDA-MB-231 breast cancer cell solution was drawn into a 1ml syringe, and the syringe was fixed on the injection pump, with the injection pump parameters set accordingly. The signal generator parameters were set to $\pm 5\text{Vrms}$ and 210kHz , and the experiment began. The formula for calculating the enrichment efficiency of the chip is as follows:

$$\text{Enrichment rate} = \frac{\text{The number of CTCs adsorbed by the electrode}}{\text{Total number of CTCs involved in separation}}$$

The experiment verified the adsorption of human breast cancer cells MDA-MB-231 (CTCs) in the chip at six different flow rates of 2.0-2.5 mL/h. Partial microscopic images are shown in Figure 7. The red boxes in the figure mark the positions of CTCs cells. From Figure a, it can be observed that when the fluid flow rate inside the chip is 2.0 mL/h, the cells are greatly affected by the dielectrophoretic force and most of the cells can be adsorbed on the bottom electrode, resulting in an enrichment efficiency of over 90%. As the flow rate increases in increments of 0.1, the breast cancer cells adsorbed on the chip gradually decrease, as the increased velocity leads to a gradual decrease in the dielectrophoretic force inside the chip. Finally, when the flow rate is increased to 2.5 mL/h, the number of MDA-MB-231 breast cancer cells that the bottom electrode can adsorb decreases significantly, making it difficult to adsorb breast cancer cells, and the enrichment efficiency drops below 20%. Figure 7d illustrates the effect of enrichment rate within the range of 2.0-2.5 mL/h.

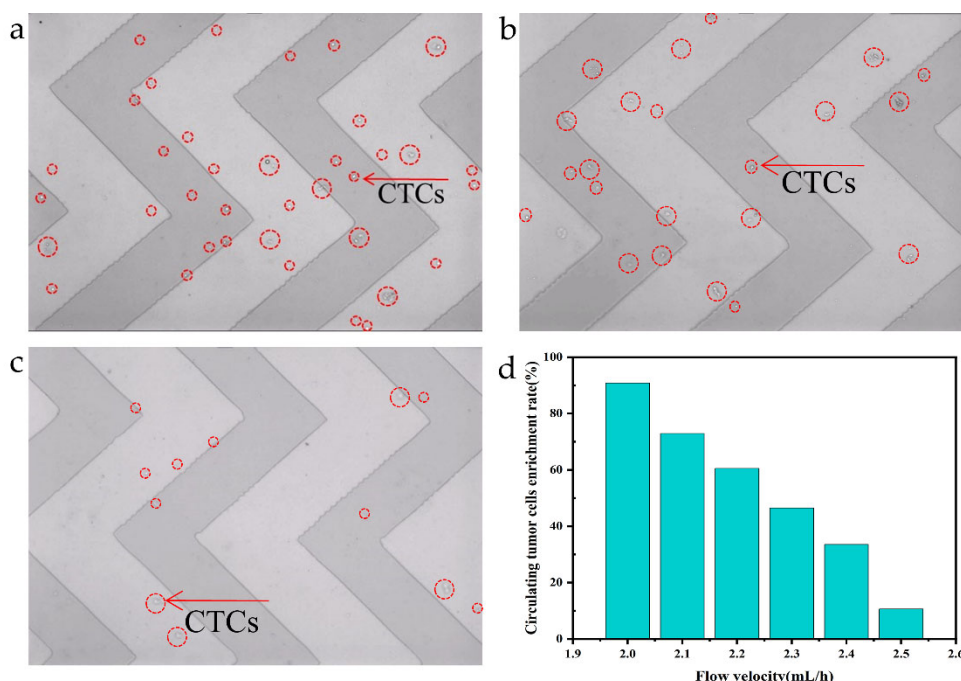


Figure 7. The adsorption situation of CTCs cells at different flow rates, the red coil is a marker of breast cancer cells, the number of which is the enrichment effect. (a) Enrichment rendering of 2.0 mL/h; (b) Enrichment rendering of 2.2 mL/h; (c) Enrichment rendering of 2.5 mL/h; (d) Efficiency chart of enriching human breast cancer cells MDA-MB-231 at different flow rates on the chip.

The experiment of white blood cell adhesion was conducted with the aforementioned parameters (210 kHz, ± 5 V_{rms}, flow rate of 2.0 mL/h), and no adhesion was observed on the chip. Subsequently, a sorting experiment was conducted with a mixture of MDA-MB-231 breast cancer cells and white blood cells, and the same sorting effect as when only breast cancer cells were sorted was achieved. Thus, it was verified that these parameters are applicable for the separation of CTCs cells from white blood cells.

4. CONCLUSIONS

We designed a zigzag three-dimensional microfluidic chip based on the principle of dielectrophoresis for sorting circulating tumor cells (CTCs) using electric field effects. For

instance, using human breast cancer cells MDA-MB-231 (CTCs) as a case study, we analyzed the impact of electrode patterns, channel height, microelectrode potential, and flow rate on cell trajectories through simulation of cell motion paths. The results showed that a zigzag electrode pattern was optimal for achieving the best simulated cell sorting effect at a channel height of 150 μm , microelectrode potential of 10V, and flow rate of 370 $\mu\text{m/s}$ (2.0 mL/h). We fabricated the electrodes and microchannels, and then bonded them using a plasma cleaning machine to prepare the chip to validate the simulation results. We further validated the optimal sorting efficiency of MDA-MB-231 human breast cancer cells by constructing a sorting experimental platform. Under the conditions of a solution conductivity of 550 $\mu\text{s/cm}$, a frequency of 210 kHz, an applied voltage of 10Vrms, and a flow rate of 2.0 mL/h, the sorting efficiency achieved its maximum level.

This study provides a novel, more cost-effective, and feasible laser etching technology for the enrichment and separation of circulating tumor cells (CTCs) via dielectrophoresis based methods. A comprehensive dataset was obtained for the sorting and enrichment of MDA-MB-231 human breast cancer cells through both simulation and experimental validation. The structure and experimental data presented in this study can serve as a valuable reference for the enrichment and detection of other types of CTCs, with only specific experimental parameters such as flow rate needing to be adjusted accordingly.

ACKNOWLEDGMENTS

This paper was supported by Key R&D Breakthrough Program of Henan Province (222102310276).

REFERENCES

- [1] Chedid, J.; Allam, S.; Chamseddine, N.; Bou Zerdan, M.; El Nakib, C.; Assi, H.I. Role of circulating tumor DNA and circulating tumor cells in breast cancer: History and updates. *SAGE open medicine* 2022, 10, 20503121221077838.
- [2] Xu, X.; Jiang, Z.; Wang, J.; Ren, Y.; Wu, A. Microfluidic applications on circulating tumor cell isolation and biomimicking of cancer metastasis. *Electrophoresis* 2020, 41, 933-951.
- [3] Miller, M.C.; Doyle, G.V.; Terstappen, L.W. Significance of circulating tumor cells detected by the cellsearch system in patients with metastatic breast colorectal and prostate cancer. *Journal of oncology* 2010, 2010, 617421.
- [4] Pei, H.; Li, L.; Han, Z.; Wang, Y.; Tang, B. Recent advances in microfluidic technologies for circulating tumor cells: Enrichment, single-cell analysis, and liquid biopsy for clinical applications. *Lab on a chip* 2020, 20, 3854-3875.
- [5] Antfolk, M.; Antfolk, C.; Lilja, H.; Laurell, T.; Augustsson, P. A single inlet two-stage acoustophoresis chip enabling tumor cell enrichment from white blood cells. *Lab on a chip* 2015, 15, 2102-2109.
- [6] Chen, Y.; Tyagi, D.; Lyu, M.; Carrier, A.J.; Nganou, C.; Youden, B.; Wang, W.; Cui, S.; Servos, M.; Oakes, K., et al. Regenerative nanooctopus based on multivalent-aptamer-functionalized magnetic microparticles for effective cell capture in whole blood. *Analytical chemistry* 2019, 91, 4017-4022.
- [7] Warkiani, M.E.; Khoo, B.L.; Wu, L.; Tay, A.K.; Bhagat, A.A.; Han, J.; Lim, C.T. Ultra-fast, label-free isolation of circulating tumor cells from blood using spiral microfluidics. *Nature protocols* 2016, 11, 134-148.
- [8] Cheng, S.-B.; Xie, M.; Xu, J.-Q.; Wang, J.; Lv, S.-W.; Guo, S.; Shu, Y.; Wang, M.; Dong, W.-G.; Huang, W.-H. High-efficiency capture of individual and cluster of circulating tumor cells by a microchip

- embedded with three-dimensional poly(dimethylsiloxane) scaffold. *Analytical chemistry* 2016, 88, 6773-6780.
- [9] Zhao, L.; Tang, C.; Xu, L.; Zhang, Z.; Li, X.; Hu, H.; Cheng, S.; Zhou, W.; Huang, M.; Fong, A., et al. Enhanced and differential capture of circulating tumor cells from lung cancer patients by microfluidic assays using aptamer cocktail. *Small (Weinheim an der Bergstrasse, Germany)* 2016, 12, 1072-1081.
- [10] Khoshmanesh, K.; Nahavandi, S.; Baratchi, S.; Mitchell, A.; Kalantar-zadeh, K. Dielectrophoretic platforms for bio-microfluidic systems. *Biosensors & bioelectronics* 2011, 26, 1800-1814.
- [11] Auerswald, J.; Knapp, H.F. Quantitative assessment of dielectrophoresis as a micro fluidic retention and separation technique for beads and human blood erythrocytes. *Microelectronic Engineering* 2003, 67-68, 879-886.
- [12] Li, M.; Li, W.; Zhang, J.; Alici, G.; Wen, W. A review of microfabrication techniques and dielectrophoretic microdevices for particle manipulation and separation. *Journal of Physics D Applied Physics* 2014, 47.
- [13] Witte, C.; Reboud, J.; Cooper, J.M.; Neale, S.L.J.o.M.; *Microengineering*. Channel integrated optoelectronic tweezer chip for microfluidic particle manipulation. 2020, 30.
- [14] Khoshmanesh, K.; Zhang, C.; Tovar-Lopez, F.J.; Nahavandi, S.; Baratchi, S.; Kalantar-zadeh, K.; Mitchell, A. Dielectrophoretic manipulation and separation of microparticles using curved microelectrodes. *Electrophoresis* 2009, 30, 3707-3717.
- [15] Grom, F.; Kentsch, J.; Müller, T.; Schnelle, T.; Stelzle, M. Accumulation and trapping of hepatitis a virus particles by electrohydrodynamic flow and dielectrophoresis. *Electrophoresis* 2006, 27, 1386-1393.
- [16] Thomas, R.S.; Morgan, H.; Green, N.G. Negative dep traps for single cell immobilisation. *Lab on a chip* 2009, 9, 1534-1540.
- [17] Krishnan, R.; Sullivan, B.D.; Mifflin, R.L.; Esener, S.C.; Heller, M.J. Alternating current electrokinetic separation and detection of DNA nanoparticles in high-conductance solutions. *Electrophoresis* 2008, 29, 1765-1774.
- [18] Li, M.; Li, S.; Wu, J.; Wen, W.; Li, W.; Alici, G. A simple and cost-effective method for fabrication of integrated electronic-microfluidic devices using a laser-patterned pdms layer. *Microfluidics and Nanofluidics* 2012, 12, 751-760.
- [19] Wang, L.; Lu, J.; Marchenko, S.A.; Monuki, E.S.; Flanagan, L.A.; Lee, A.P. Dual frequency dielectrophoresis with interdigitated sidewall electrodes for microfluidic flow-through separation of beads and cells. *Electrophoresis* 2009, 30, 782-791.
- [20] Yoshioka, J.; Ohsugi, Y.; Yoshitomi, T.; Yasukawa, T.; Sasaki, N.; Yoshimoto, K. Label-free rapid separation and enrichment of bone marrow-derived mesenchymal stem cells from a heterogeneous cell mixture using a dielectrophoresis device. *Sensors (Basel, Switzerland)* 2018, 18.
- [21] Wu, Y.; Ren, Y.; Tao, Y.; Hou, L.; Jiang, H. High-throughput separation, trapping, and manipulation of single cells and particles by combined dielectrophoresis at a bipolar electrode array. *Analytical chemistry* 2018, 90, 11461-11469.
- [22] Luo, T.; Fan, L.; Zeng, Y.; Liu, Y.; Chen, S.; Tan, Q.; Lam, R.H.W.; Sun, D. A simplified sheathless cell separation approach using combined gravitational-sedimentation-based prefocusing and dielectrophoretic separation. *Lab on a chip* 2018, 18, 1521-1532.